ISSN 1068-3356, Bulletin of the Lebedev Physics Institute, 2023, Vol. 50, No. 11, pp. 473–479. © Allerton Press, Inc., 2023.
Russian Text © The Author(s), 2023, published in Kratkie Soobshcheniya po Fizike, 2023, Vol. 50, No. 11, pp. 30–40.

Observation of Parametric X-Ray Radiation from Highly Oriented Pyrolytic Graphite in Backscattering Geometry

I. A. Kishin[a,b,*], E. Yu. Kidanova[a], A. S. Kubankin[a,b], R. M. Nazhmudinov[a,b,c], V. I. Alekseev[b], and A. N. Eliseev[b]

[a] *Belgorod State National Research University, Belgorod, 308015 Russia*

[b] *Lebedev Physical Institute, Russian Academy of Sciences, Moscow, 119991 Russia*

[c] *Shukhov Belgorod State Technological University, Belgorod, 308012 Russia*

**e-mail: ivan.kishin@mail.ru*

Received September 19, 2023; revised September 28, 2023; accepted September 29, 2023

Abstract—The paper presents the results of an experiment on the generation of parametric X-ray radiation (PXR) in the interaction of relativistic electrons with highly oriented pyrolytic graphite. The measurements are performed at an observation angle of 180° relative to the electron velocity. For the first time, the spectrum of parametric X-ray radiation formed in highly oriented pyrolytic graphite in the backscattering geometry was recorded. The dependences of the radiation output on the orientation angle of the irradiated target are measured.

Keywords: parametric X-ray radiation, highly oriented pyrolytic graphite, relativistic electrons, X-ray source

DOI: 10.3103/S1068335623110064

1. INTRODUCTION

Parametric X-ray radiation (PXR) is coherent radiation formed in a medium with ordered structure upon exposure to beams of accelerated charged particles. Of particular interest is PXR of relativistic electrons, since this radiation type makes it possible to develop an intense source of quasi-monochromatic X-rays with tunable energy [1]. Throughout several years, theoretical and experimental studies devoted to PXR properties and its possible applicability considered crystals [2], polycrystals [3], metamaterials [4], and powders [5, 6] as targets. The possibility of using PXR for diagnostics of charged particle beams [7], the study of the structure of biological objects [8], X-ray tomography [9], and the study of characteristics of emitting targets [10] was shown.

Currently, there are two stations using PXR as a basic mechanism for generation X-rays. The LEBRA-PXR station [8] makes it possible generate quasi-monochromatic radiation in the energy range of from 4 to 33 keV during the interaction of a 100-MeV electron beam with a silicon crystal. The second similar station [4] allows generation of radiation with energies from 60 to 300 eV by using Van der Waals structures as targets.

The main disadvantage of commercial sources based on PXR is a rather low intensity of generated radiation. The prospect of the use of highly oriented pyrolytic graphite (HOPG) as a target material was considered to solve this problem [11–13]. This target type has not an ideal structure, and is a mosaic crystal.

Such a crystal provides a higher yield of X-ray radiation in comparison with a perfect crystal, which was demonstrated theoretically [14]. Powder targets and polycrystals are not considered as targets for PXR sources because of a very low radiation yield [15, 16].

In this paper, we present the results of an experiment in which PXR of relativistic electrons, formed in HOPG in the backscattering geometry was detected for the first time. The measured X-ray spectra contain high-order PXR peaks, which was also observed in previous studies [17, 18]. In the present study, the energy and the full width at half-maximum of PXR spectral peaks were determined.

A new measurement technique was proposed and an experiment was described, in which the dependences of the PXR yield on the target orientation angle were obtained.

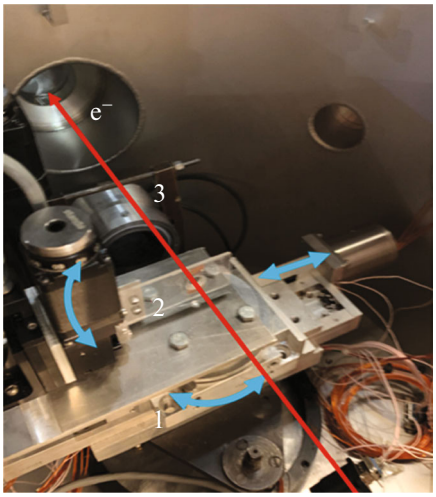

Fig. 1. Photograph of elements placed within the target chamber: (1) goniometer, (2) frame for fixing the target, (3) Faraday cup in the off position.

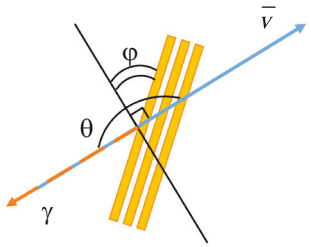

Fig. 2. Experimental geometry. θ is the observation angle, φ is the target orientation angle.

2. EXPERIMENTAL SETUP

Measurements were performed on the "Rentgen 1" experimental setup [19] of the Lebedev Physical Institute (LPI).

As a source of relativistic electrons, a microtron with a beam energy of 7 MeV, a beam dump frequency of 50 Hz, and a dump duration to 4 μs was used.

As a target, HOPG with a mosaicity of $0.4° \pm 0.1°$ and $10 \times 10 \times 1$ mm in size was used. The target was fixed on a plexiglas frame (2) (see Fig. 1) placed on a goniometer (1) allowing target rotation revolution about vertical and horizontal axes with an accuracy of $\pm 0.01°$ which was sufficient for measurements.

The goniometer was installed in the vacuum chamber, the working pressure in which during the experiment was 10^{-5} Torr.

The beam intensity was measured with a Faraday cup (3) and a nanoamperemeter; the measured average current was in the range of 1–10 nA. The beam position, size, and shape were determined using a gas-filled proportional chamber. The beam size was 3 mm with an initial divergence of 15 mrad.

PXR spectra were measured at an observation angle $\theta = 180°$, i.e., in such geometry when measured radiation propagates in the opposite direction with respect to the incident electron velocity vector (see Fig. 2). The angle φ corresponds to the target orientation angle.

Emission spectra were measured using an Amptek X-123SDD X-ray spectrometer [18]. The spectrometer calibration and the determination of its energy resolution under experimental conditions were performed by the measured characteristic X-ray (CXR) spectra of silicon ($K_\alpha = 1.740$ keV), the titan (titanium) ($K_\alpha = 4.510$ keV), nickel ($K_\alpha = 7.478$ keV), and platinum ($L_\alpha = 9.442$ keV) at a shaping time of 1 μs. Samples for calibration were placed instead of the target. The spectrometer energy resolution was 98–177 eV in the energy range of 1–10 keV. The radiation emission beam light detection efficiency in the energy range from 1.5 to 10 keV is within 70–100% (see Fig. 3).

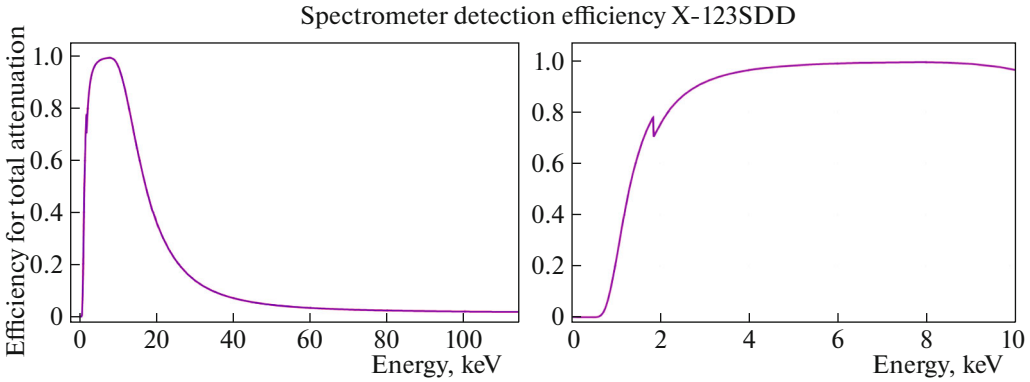

Fig. 3. Detection efficiency of radiation by the X-123SDD spectrometer; the data for constructing the curve are taken from the manufacturer site [20]. The left panel shows the curve for all spectral energy range. The right panel shows the curve for the energy range of interest.

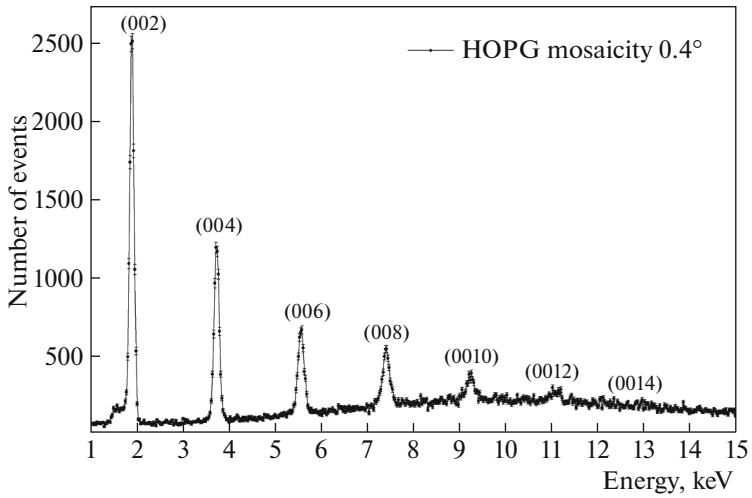

Fig. 4. Primary spectrum of PXR from HOPG with a mosaicity of 0.4°.

The spectrometer was surrounded by lead protection and was rigidly collimated by a tungsten collimator with an aperture of 1 mm and a lead collimator with an aperture of 5 mm so that the detector would "see" only the target. The solid angle was 3.22×10^{-7} sr. The signal formation time in all the experiments was 1 μs.

3. MEASUREMENTS

The first experiments revealed six diffraction orders from crystallographic planes of the series (00N), where N = 2, 4, 6, ... in the spectra. Figure 4a shows the PXR spectrum of HOPG measured during the experiment.

The PXR peak positions measured and calculated by the Bragg formula are listed in Table 1. The calculated values were obtained under the following conditions: the observation angle $\theta = 180°$, the lattice is hexagonal (alpha graphite) with the parameters $a = 1.418$ Å and $c = 6.71$ Å. As seen in Fig. 4 and Table 1, there is good agreement of spectral peak positions for all crystallographic planes.

The measured PXR peaks during experimental data processing were approximated by the Gaussian function, after which spectral widths at half-maximum were calculated. The calculated results are listed in Table 2. We can see that the width at half-maximum of PXR peaks is comparable to the detector energy resolution in the spectral region under study; an insignificant excess is observed for the third and fourth orders, which is associated with poor statistics of the experimental data set. For higher diffraction orders,

Table 1. Calculated and experimental PXR peak positions from HOPG

Crystallographic plane	Calculated PXR, keV	Experimental PXR, keV
(002)	1.859	1.869 ± 0.001
(004)	3.718	3.720 ± 0.002
(006)	5.576	5.564 ± 0.003
(008)	7.435	7.409 ± 0.008
(00 10)	9.294	9.266 ± 0.007
(00 12)	11.153	11.106 ± 0.012
(00 14)	13.012	12.979 ± 0.039

Table 2. Spectral widths of peaks PXR at half maximum (FWHM)

Plane	Energy, eV	
	Full width at half-maximum	Spectrometer energy resolution
(002)	111 ± 0.7	109 ± 1
(004)	127 ± 1.7	127 ± 2
(006)	159 ± 4.2	144 ± 6
(008)	183 ± 7.0	159 ± 10

widths at half-maximum were not calculated in view of an insufficient statistics. Based on the presented data, we can say that the spectral line broadening due to mosaicity was not observed. At the same time, in [21], among two most appropriate HOPG and LiF targets, to achieve the optimum radiation yield, LiF was chosen, since HOPG exhibits PXR line broadening. It is possible that the difference between the results obtained is associated with the chosen observation geometry. It is known that the spectral width is minimum in the backscattering geometry [22, 23].

However, during the experiment, in attempts to obtain the dependence of the PXR yield on the target orientation angle, similar to the "rocking curve" in X-ray spectroscopy, the problem arose: the beam intensity varied from 1 to 10 nA. To solve this problem, the normalization to the CXR target intensity proportional to the beam current is used in some experiments with crystals and polycrystals. An X-123SDD spectrometer with an input beryllium window 12.5 μm thick was used in the experiment, which does not allow observation of radiation with energies lower than 677 eV. Since the characteristic K_α carbon line energy is 277 eV which is below the possible detection energy for the used spectrometer, the normalization of results to the carbon CXR seems impossible.

According to the calculation of the position of PXR peaks from HOPG, an optimum case is the normalization to the copper CXR lines which are close to the energies $K_\alpha = 8.048$ keV and $K_\beta = 8.905$ keV.

An advantage of the use of copper in this experiment is also total absorption of copper $L_\alpha = 0.93$ keV and partial absorption of copper K_α in HOPG 1 mm thick, which makes it possible not to overload the detector used in the experiment.

For the purpose of normalization, the copper foil 40 μm thick was tightly fixed to the HOPG target surface output for the electron beam. The normalization was performed by measuring the copper K_α line intensity. Figure 5 shows the PXR spectrum formed in HOPG with a mosaicity of 0.4° after placing the copper foil. There are clearly seen PXR reflections from (002), (004), (006), (008) planes; there are also peaks of characteristic copper K_α and K_β lines. It should be noted that the copper CXR and PXR yields from HOPG are comparable, whereas, e.g., in experimental studies [24, 16], it was shown that the PXR yield from polycrystals is several orders of magnitude lower than the CXR yield from the target.

After placing a copper foil, the orientation dependences of the PXR yield in the horizontal plane were measured. The results obtained are shown as a heat map in Fig. 6. The two-humped angular distribution with a dip at a target orientation angle $\varphi = 0°$ is observed, which is typical of PXR formed in crystalline targets.

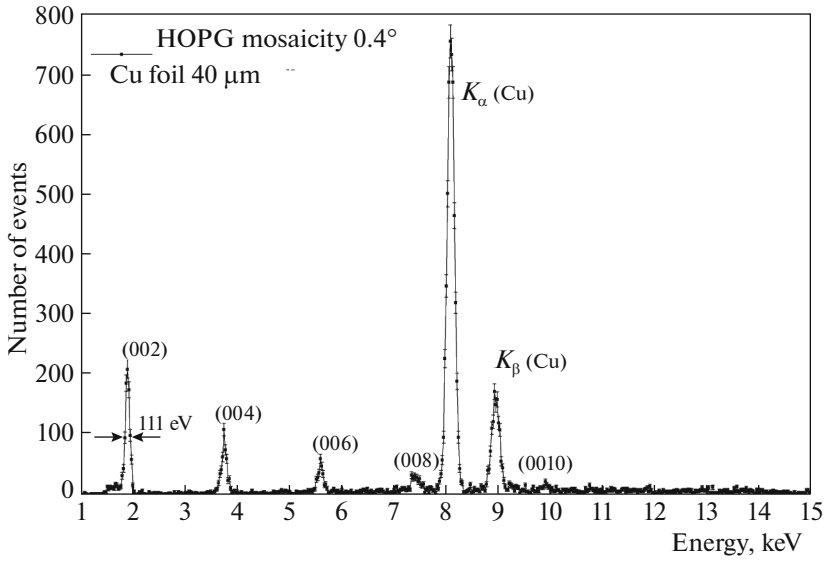

Fig. 5. Spectrum of PXR from HOPG with a mosaicity of 0.4° after placing a copper target.

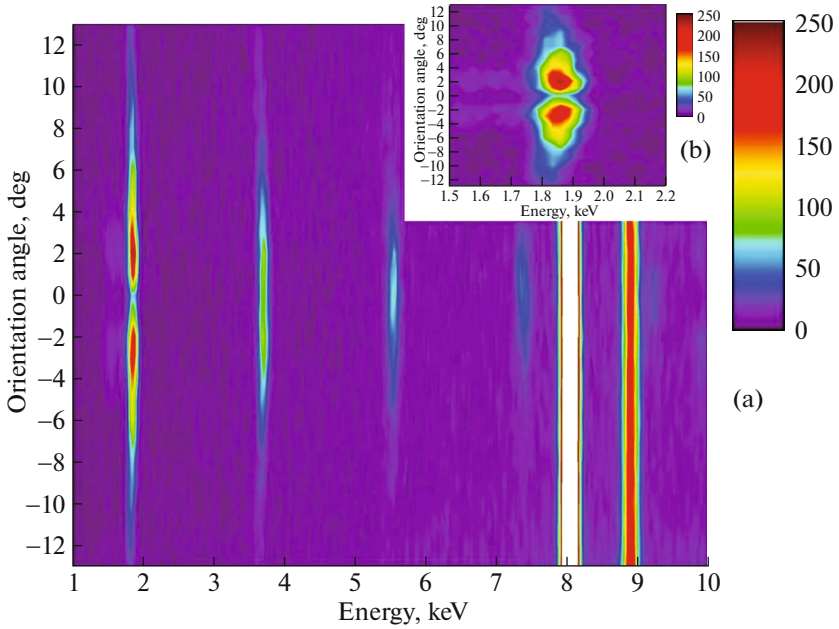

Fig. 6. Dependences of PXR yield intensity on the target orientation angle φ. (a) Energy range from 1 to 10 keV, (b) energy range from 1.5 to 2.2 keV.

Radiation yield maxima are observed at angle $\varphi_{max} = \pm 2°$. The maximum PXR yield angle can be determined by the formula

$$\varphi_{max} = \frac{1}{2\gamma_{eff}} = \frac{\sqrt{\gamma^{-2} + \frac{\omega_0^2}{\omega^2}}}{2},$$

where γ is the electron Lorentz factor, ω_0 is the plasma frequency, and ω is the radiation energy. The factor of two in the denominator of this formula is caused by the measurement geometry used in the experiment, in which a crystal rotation by angle φ causes a PXR beam deflection in space by angle 2φ. Therefore, the

measured angular dependence of the radiation yield appears "compressed" relative to angular coordinates.

As seen in Fig. 6, the dip is explicitly observed for the first-order diffraction and is insignificant for the second order; for other orders, orientation dependences are narrowed. We can see that the dip at 0° is "smeared"; this phenomenon is associated with multiple scattering of electrons in the target under study.

4. CONCLUSIONS

PXR formed during the interaction of a 7-MeV electron beam with highly oriented pyrolytic graphite was experimentally studied.

(i) It was possible to reliably detect six PXR reflections from the 002 plane for the observation angle of 180° and the electron energy of 7 MeV.

(ii) It was found that widths at half-maximum of observed PXR reflections do not exceed the detector energy resolution for the first and second diffraction orders in the observed spectral region.

(iii) The measured orientation dependences of the PXR yield on the target orientation angle showed a typical two-humped angular distribution for crystalline targets only for the first-order diffraction from the (002) plane.

FUNDING

This work was financially supported by a Program of the Ministry of Education and Science of the Russian Federation for higher education establishments, project no. FZWG-2020-0032 (2019–1569). The work was carried out with the support of from the President of the Russian Federation for young scientists-Candidates of Sciences, grant no. MK- 1320.2022.1.2.

CONFLICT OF INTEREST

The authors of this work declare that they have no conflicts of interest.

REFERENCES

1. Hyun, J., Satoh, M., Yoshida, M., et al., Compact and intense parametric x-ray radiation source based on a linear accelerator with cryogenic accelerating and decelerating copper structures, *Phys. Rev. Accel. Beams,* 2018, vol. 21, p. 014701. https://doi.org/10.1103/PhysRevAccelBeams.21.014701
2. Baryshevsky, V.G., Spontaneous and induced radiation by electrons/positrons in natural and photonic crystals. Volume free electron lasers (VFELs): From microwave and optical to X-ray range, *Nucl. Instrum. Methods Phys. Res. B,* 2015, vol. 355, pp. 17–23. https://doi.org/10.1016/j.nimb.2015.04.004
3. Blazhevich, S., Chepurnov, A., Grishin, V., et al., Polarization bremsstrahlung of relativistic electrons in aluminium, *Phys. Lett. A,* 1999, vol. 254, pp. 230–232. https://doi.org/10.1016/S0375-9601(99)00056-0
4. Shentcis, M., Budniak, A.K., Shi, X., et al., Tunable free-electron X-ray radiation from van der Waals materials, *Nat. Photonics,* 2020, vol. 14, pp. 686–692. https://doi.org/10.1038/s41566-020-0689-7
5. Alekseev, V.I., Eliseyev, A.N., Irribarra, E., et al., Parametric X-ray radiation from powders, *Phys. Lett. A,* 2019, vol. 383, pp. 770–773. https://doi.org/10.1016/j.physleta.2018.11.044
6. Alekseev, V.I., Eliseev, A.N., Kishin, I.A., et al., Effect of the grain size of powder targets on the spectra of parametric X-ray radiation of relativistic electrons, *Bull. Lebedev Phys. Inst.,* 2021, vol. 48, pp. 35–40. https://doi.org/10.3103/s1068335621020056
7. Skoromnik, O.D., Feranchuk, I.D., and Lu, D.V., Parametric X-ray radiation in the Smith–Purcell geometry for non-destructive beam diagnostics, *Nucl. Instrum. Meth. B,* 2019, vol. 444, pp. 125–134. https://doi.org/10.1016/j.nimb.2019.01.003
8. Hayakawa, Y., Takahashi, Y., Kuwada, T., et al., X-ray imaging using a tunable coherent X-ray source based on parametric X-ray radiation, *J. Instrum.,* 2013, vol. 8, C08001. https://doi.org/10.1088/1748-0221/8/08/C08001

9. Hayakawa, Y., Hayakawa, K., Nogami, K., et al., Performance of K-edge subtraction tomography as an application of parametric x-ray radiation, *Phys. Rev. Accel. Beams,* 2019, vol. 22, p. 024701. https://doi.org/10.1103/PhysRevAccelBeams.22.024701
10. Nasonov, N., Zhukova, P., and Sergienko, V., Polarization bremsstrahlung in a backward direction for medium structure diagnostics, *J. Phys. Conf,* 2010, vol. 236, p. 012017. https://doi.org/10.1088/1742-6596/236/1/012017
11. Bogomazova, E.A., Kalinin, B.N., Naumenko, G.A., et al., Diffraction of real and virtual photons in a pyrolytic graphite crystal as source of intensive quasimonochromatic X-ray beam, *Nucl. Instrum. Methods Phys. Res. B,* 2002, vol. 201, pp. 276–291. https://doi.org/10.1016/S0168-583X(02)01435-0
12. Vnukov, I.E., Zhandarmov, Yu.V., and Shatokhin, R.A., X-ray source with variable photon's energy for medicine applications, *Visnik Kharkivskogo Universitetu,* 2008, vol. 808, p. 25.
13. Baklanov, D.A., Baldin, A.N., Vnukov, I.E., et al., Relation contribution of diffracted bremsstrahlung and parametric X-ray radiation in perfect crystals, *Visnik Kharkivskogo Universitetu,* 2007, vol. 763, p. 41.
14. Artru, X. and Rullhusen, P., Parametric X-rays and diffracted transition radiation in perfect and mosaic crystals, *Nucl. Instrum. Methods B*, 1998, vol. 145, no. 1–2, pp. 1–7. https://doi.org/10.1016/S0168-583X(98)00241-9
15. Kishchin, I.A., Kidanova, E.Yu., Kubankin, A.S., et al., Generation of parametric X-ray radiation from ultrafine powder of burnt magnesia, *Bull. Lebedev Phys. Inst.,* 2022, vol. 49, pp. 401–406. https://doi.org/10.3103/S106833562212003X
16. Alekseev, V.I., Eliseev, A.N., Irribarra, E.F., et al., Research of the polarization bremsstrahlung of relativistic electrons in polycrystalline targets, *Nucl. Instrum. Methods Phys. Res. B,* 2015, vol. 342, pp. 47–51. https://doi.org/10.1016/j.nimb.2014.09.009
17. Fiorito, R.B., Rule, D.W., Maruyama, X.K., et al., Observation of higher order parametric X-ray spectra in mosaic graphite and single silicon crystals, *Phys. Rev. Lett.,* 1993, vol. 71, pp. 704–707. https://doi.org/10.1103/PhysRevLett.71.704
18. Amosov, K.Yu., Andreyashkin, M.Yu., Verzilov, V.A., et al., Parametric X-radiation in a mosaic crystal of pyrolytic, *JETP Lett.,* 1994, vol. 60, no. 7, pp. 506–510.
19. Alexeyev, V.I., Astapenko, V.A., Eliseyev, A.N., et al., Investigation into the mechanisms of X-ray generation during the interaction between relativistic electrons and a medium by means of the Röntgen-1 setup, *J. Surf. Invest.,* 2017, vol. 11, no. 4, pp. 694–698. https://doi.org/10.1134/S1027451017040036
20. Amptek, FAST SDD Ultra High-Performance Silicon Drift Detector. https://www.amptek.com/products/x-ray-detectors/fastsdd-x-ray-detectors-for-xrf-eds/fastsdd-silicon-drift-detector
21. Sones, B., Danon, Y., and Block, R.C., Lithium fluoride (LiF) crystal for parametric X-ray (PXR) production, *Nucl. Instrum. Methods Phys. Res. B,* 2005, vol. 227, pp. 22–31. https://doi.org/10.1016/j.nimb.2004.05.008
22. Astapenko, V., Nasonov, N., and Zhukova, P., Anomalous peak in the spectrum of polarizational bremsstrahlung from relativistic electrons moving through a solid target, *J. Phys. B,* 2007, vol. 40, pp. 1337–1346. https://doi.org/10.1088/0953-4075/40/7/003
23. Alekseev, V.I., Eliseyev, A.N., Irribarra, E., et al., Evolution of the characteristics of parametric X-ray radiation from textured polycrystals under different observation angles, *Phys. Lett. A,* 2018, vol. 382, pp. 503–506. https://doi.org/10.1016/j.physleta.2017.12.038
24. Alekseev, V.I., Eliseyev, A.N., Irribarra, E., et al., Parametric X-ray radiation from nanopowders, *Radiat. Phys. Chem.,* 2023, vol. 202, p. 110497. https://doi.org/10.1016/j.radphyschem.2022.110497

Translated by A. Kazantsev